

# Size Effect on Microstructural Evolution and Micromechanical Responses of Mechanically Bonded Aluminum and Magnesium by High-Pressure Torsion

Jae-Kyung Han, Jeong-Min Park, Wei Ruan, Kevin T. Carpenter, Ali Tabei, Jae-il Jang, and Megumi Kawasaki\*

The mechanical bonding of dissimilar metals through the application of high-pressure torsion (HPT) processing is developed recently for introducing unique ultrafine-grained alloy systems involving microstructural heterogeneity leading to excellent mechanical properties. Considering further developments of the processing approach and the produced hybrid materials, the size effect on microstructural evolution and micromechanical responses of the mechanically bonded Al–Mg systems is evaluated. In practice, processing by HPT is conducted at room temperature on the separate Al and Mg disks having 25 mm diameter under 1.0 GPa at 0.4 rpm, and the results are compared with the mechanically bonded Al–Mg system having 10 mm diameter. The Al–Mg disks having 25 mm diameter show a general hardness distribution where low hardness appears around the disk centers, and it increases at the disk peripheries. Nanoindentation measurements demonstrate that there is excellent plasticity at the edges of the Al–Mg system with 25 mm diameter. The Al–Mg system with both 10 and 25 mm diameters show a consistent trend of hardness evolution outlining an exponential increase of hardness with increasing equivalent strain. The results are anticipated to provide a conceptual framework for the development and scale-up of the HPT-induced mechanical bonding technique.

considerable amounts of point and line defects promoting fast atomic mobility during processing generally at ambient temperatures. Accordingly, the application of HPT processing has been extended for the bonding of machining metal chips<sup>[4–7]</sup> and the consolidation of metallic powders<sup>[8–17]</sup> as well as for the solid-state recycling.<sup>[18]</sup>

Considering the ability of HPT processing for the solid-state reactions, several recent studies demonstrated the successful demonstrations of the mechanical bonding of dissimilar bulk metals by utilizing the conventional HPT procedure with applying a unique sample set-up. In practice, two dissimilar metallic disks having a diameter of 10 mm are prepared and placed alternately without applying any gluing procedure on the lower anvil for the regular HPT processing procedure, and these are schematically shown in Figure 1a,b. While an unlimited number of material combinations are available, this approach was often applied for nonferrous metals and alloys to improve their upper limits of mechanical

## 1. Introduction

The significance of a high-pressure torsion (HPT) technique has been recognized for processing of true bulk nanocrystalline materials over the last two decades.<sup>[1,2]</sup> As described earlier,<sup>[3]</sup> an HPT technique applies a very high compressive pressure and concurrent severe torsional straining to a bulk material in the shape of a disk. The HPT-processed materials receive

properties by microstructural refinement with maintaining constant or further lowering the density of the material systems by a severe microstructural mixture. Thus, numerous studies were reported for the mechanical bonding of the combinations of Al and Cu<sup>[19–22]</sup> and Al and Mg<sup>[23–27]</sup> and demonstrated the evolution of microstructure and chemical compositions and enhancement in mechanical properties.


In principles of HPT processing, an apparent limitation in HPT processing is that torsional straining introduced within the HPT disk is markedly inhomogeneous and generally radially symmetrical. Specifically, when a disk material is processed in such conventional HPT, the equivalent strain,  $\epsilon_{eq}$ , is given by a relationship of the form<sup>[28,29]</sup>

$$\epsilon_{eq} = \frac{2\pi Nr}{\sqrt{3}h} \quad (1)$$

where  $N$  is the number of revolutions and  $r$  and  $h$  are the radius and height (or thickness) of the disk, respectively. Thus, such heterogeneous distribution of torsional straining influences significantly the mechanical bonding and the introduction of intermetallic phases by the severe mixture of the dissimilar

J.-K. Han, W. Ruan, K. T. Carpenter, Prof. A. Tabei, Prof. M. Kawasaki  
School of Mechanical, Industrial and Manufacturing Engineering  
Oregon State University  
Corvallis, OR 97331, USA  
E-mail: megumi.kawasaki@oregonstate.edu

J.-M. Park, Prof. J.-i. Jang  
Division of Materials Science and Engineering  
Hanyang University  
Seoul 04763, Republic of Korea

 The ORCID identification number(s) for the author(s) of this article can be found under <https://doi.org/10.1002/adem.201900971>.

DOI: 10.1002/adem.201900971

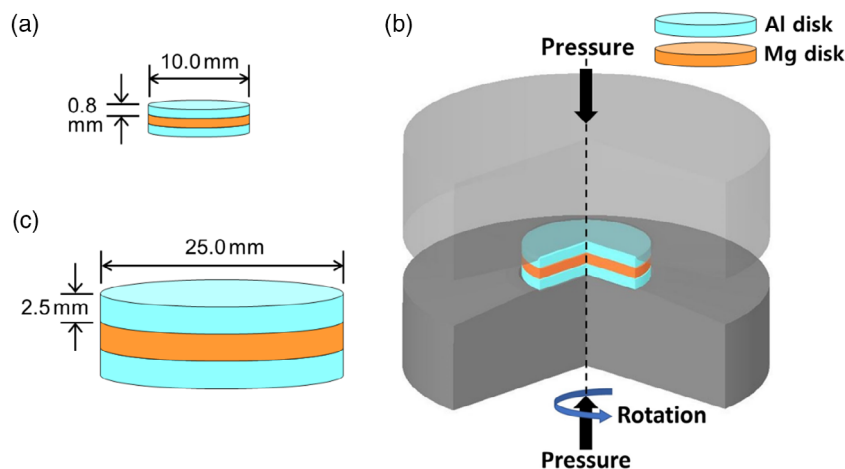


**Figure 1.** Schematic drawings of a) a sample set-up with disks having 10 mm diameter, b) HPT processing for the mechanical bonding, and c) a sample set-up with disks having 25 mm diameter.

metals. Limited reports are available to date demonstrating a scaling-up approach of the HPT sample sizes in terms of a disk thickness,<sup>[30]</sup> an  $r/h$  ratio,<sup>[31]</sup> and microstructural homogeneity<sup>[32]</sup> when processing was conducted on a simple metal. However, there is no report demonstrating HPT processing for the mechanical bonding of dissimilar metals in large sample sizes.

Accordingly, the present study was initiated to demonstrate the mechanical bonding by HPT of large Al and Mg disks having a diameter of 25 mm as schematically shown in Figure 1c. Moreover, experiments are conducted to evaluate the evolution of microstructure and hardness, examine the micromechanical responses of the scaled-up Al–Mg system, and compare the system with the Al–Mg system having a disk diameter of 10 mm. The results in this study are anticipated to provide a conceptual framework for the development and scale-up of the HPT-induced mechanical bonding technique and to develop strategies for tailoring the desirable microstructural formation in bulk nanocrystalline metals.

## 2. Experimental Section

For the synthesis of a large-sized Al–Mg alloy system, two conventional metals were prepared: a commercial purity Al (Al-1050) containing 0.40 wt% Fe and 0.25 wt% Si as a major impurity with <0.07 wt% Zn and <0.05 wt% of Cu and Mg as a minor impurity and a commercial AZ 31 magnesium alloy containing 3 wt% Al and 1 wt% Zn. A plate of the Al with a thickness of 3.0 mm was cut into disks with diameters of  $\approx 25$  mm by electric discharge machining. The Mg alloy was received as extruded bars having diameters of 25 mm and these were sliced into disks with thicknesses of  $\approx 3.0$  mm. The disks of Al and Mg were then polished to have final parallel thicknesses of  $\approx 2.5$  mm.

These disks were processed by HPT with a sample set-up as shown in Figure 1c, where the dissimilar metals are stacked in the order of Al/Mg/Al without any surface treatment. HPT processing was conducted under 1.0 GPa at room temperature for 10 and 20 turns at a rotational speed of 0.4 rpm. This torsional

speed was selected for the 25 mm diameter disks to introduce an equivalent speed of 1.0 rpm at the disk periphery of a 10 mm diameter disk. Moreover, a reduction in torsional speed can avoid the heat generation during processing where the temperature rise is more pronounced when the sample diameter increases.<sup>[32]</sup> Final total thicknesses of the processed disk is  $\approx 2.4$  mm for both 10 and 20 turns.

The Al–Mg disks with 25 mm diameter after HPT processing were cut into half along the disk diameter, and the cross-sectional surfaces of the semi-circle disks were polished mechanically to achieve mirror-like conditions using colloidal silica suspension. The polished vertical cross sections of the Al–Mg disks were examined for the Vickers microhardness with a tester, Mitutoyo HM-200, equipped with an optical microscope. After taking a series of optical micrographs of the overall cross-sectional surfaces, the Vickers microhardness values were measured with intervals of 0.2 mm in a grid pattern at a load of 100 gf (0.98 N) and a dwell time of 10 s. The Vickers microhardness values of the base materials of Al and Mg without processing were  $\approx 20$  and  $\approx 72$ , respectively.

Microstructural analysis was conducted using transmission electron microscopy (TEM), JEOL JEOM-2100 F, at the edge of the 25 mm disk processed by HPT for 20 turns. The TEM specimens were prepared using a focused ion beam (FIB), FEI Quanta 3D FEG, where the samples were taken along the disk thickness direction at the disk edge at  $r \approx 10$  mm so as to study the microstructure facing to the radial direction of the Al–Mg disk. Crystallographic analyses were conducted at the near-center ( $2.5 \text{ mm} < r < 3.5 \text{ mm}$ ), mid-radius ( $6.0 \text{ mm} < r < 7.0 \text{ mm}$ ), and edge ( $9.5 \text{ mm} < r < 10.5 \text{ mm}$ ) regions within the disks after HPT for 10 and 20 turns by micro X-ray diffraction ( $\mu$ XRD) utilizing a Bruker D8-Discover using a conical shape slit with area of  $1.0 \text{ mm}^2$  and Cu  $K\alpha$  radiation at a scanning speed and a step interval of  $1^\circ \text{ min}^{-1}$  and  $0.01^\circ$  for 10 turns and  $2^\circ \text{ min}^{-1}$  and  $0.03^\circ$  for 20 turns, respectively, due to an instrumental limitation. Each  $\mu$ XRD measurement was taken at  $\approx 0.3$  mm from a slightly grinded disk surface. The changes in the crystal structure, lattice parameter, microstrain, and crystallite size were

examined using XRD data analysis software, materials analysis using diffraction (MAUD),<sup>[33]</sup> based on Rietveld analysis.

The micromechanical responses were examined at the disk edges of  $r \approx 10$  mm in the Al–Mg system after HPT for 10 and 20 turns using a nanoindentation facility, Nanoindenter-XP (formerly MTS; now Keysight, Santa Rosa, CA) with a three-sided pyramidal Berkovich indenter having a centerline-to-face angle of  $65.3^\circ$ . For better statistical validity, more than 15 indentations were conducted at the peripheries of the disks at each indentation strain rate. A predetermined peak applied load of  $P_{\max} = 50$  mN was applied for all measurements at constant indentation strain rates,  $\dot{\epsilon}_i$  of 0.0125, 0.025, 0.05, and  $0.1 \text{ s}^{-1}$ , where, referring to an empirical relationship, these are equivalent to general strain rates,  $\dot{\epsilon}$ , of  $1.25 \times 10^{-4}$ ,  $2.5 \times 10^{-4}$ ,  $5.0 \times 10^{-4}$ , and  $1.0 \times 10^{-3} \text{ s}^{-1}$ .

### 3. Results

#### 3.1. Overall Microstructure and Hardness Development

It is reasonable to briefly review the mechanically bonded Al–Mg system through HPT when using the 10 mm diameter disks of Al and Mg. **Figure 2** shows a) an overview of the disk cross sections with the corresponding hardness contour maps for the Al–Mg alloy having 10 mm diameter synthesized by HPT for 1, 10, and 20 turns at 6.0 GPa and b) a TEM micrographs taken at the disk edge after 20 HPT turns.<sup>[26,27]</sup> Figure 2a shows that the demonstration is valid because of the radial symmetry of the microstructural and hardness development during HPT. The microstructure and hardness variations show the change from the simple bonding of Al and Mg throughout the disk diameter after 1 turn toward necking of the Al and Mg phases at the disk centers and severe mixture of these phases at the disk edges after 10 and 20 turns. Moreover, nucleation of intermetallic compounds was observed at the disk peripheral region<sup>[26,27]</sup> receiving severe straining so that the hardness increased significantly with increasing numbers of HPT turns up to 20. An average grain size of  $\approx 60$  nm was observed in a reasonably equiaxed matrix Al as shown in Figure 2b, while some edge region formed a layered microstructure with thicknesses of the layers of 20 nm.<sup>[26]</sup>

A similar presentation of the cross-sectional micrographs and the corresponding hardness distributions as color-coded contour maps are shown in **Figure 3a** for the large Al–Mg disks with

25 mm diameter after processing by HPT for 10 turns (upper) and 20 turns (lower) under 1.0 GPa at 0.4 rpm, and the hardness valuation with the standard error against the disk diameter is shown in Figure 3b for these two mechanically bonded Al–Mg disks having 25 mm diameter. A brighter region represents an Al-rich phase, a darker phase represents a Mg-rich phase in the micrographs, and the hardness scale in Figure 3a is consistent with the one used for the Al–Mg disks having 10 mm diameter as shown in Figure 2a.

There are two notable features shown in Figure 3. First, the observed microstructure involves an apparent gradation and it is radial symmetry in the 25 mm diameter disks after HPT. In practice, large fragments of the Mg phases exist at  $r \leq 7$  mm around the mid-height of the disk thickness, and small Mg phases are visible at the remaining disk peripheral region of  $r \geq 7$  mm after 10 HPT turns. Additional HPT turns to 20 tends to reduce the presence of the large Mg phases at  $r \leq 5$  mm, and the small Mg phases exist at  $5 < r < 10$  mm, but there is no visible Mg phase at  $r > 10$  mm. Second, a general hardness behavior involving lower hardness at the disk center and high hardness at the disk periphery is observed within the mechanically bonded Al–Mg disks with 25 mm diameter, and the high hardness at the disk edge increases with an increasing numbers of HPT turns from 10 to 20 at 1.0 GPa. Specifically, as shown in Figure 3b, a central region at  $r \leq 7$  mm shows the Vickers microhardness value of  $\approx 50$ , which gradually increases toward the disk edge to have hardness of  $\approx 100$ – $110$  after HPT for 10 turns. The highest hardness of  $\approx 100$ – $110$  is consistent with the saturated hardness value for the Mg alloy after HPT for 5 turns or higher.<sup>[34]</sup> Processing by HPT for 20 turns failed to increase the low hardness value at the disk center at  $r < 5$  mm, but hardness gradually increases to demonstrate the highest hardness of  $\approx 250$  at one of the disk edge in the measured cross section, whereas the other end of the disk edge shows as low as  $\approx 180$ . The hardness difference at different peripheral regions within a disk is attributed to the misalignment of the HPT anvils during processing especially for higher numbers of turns.<sup>[35,36]</sup>

A comparison between Figure 2 and 3 reveals that an absence of the large Mg phases near the disk centers in the Al–Mg system with 25 mm diameter leads to a failure of constructing multilayered microstructure where the multilayers are visible consistently at the disk centers in the Al–Mg system with 10 mm

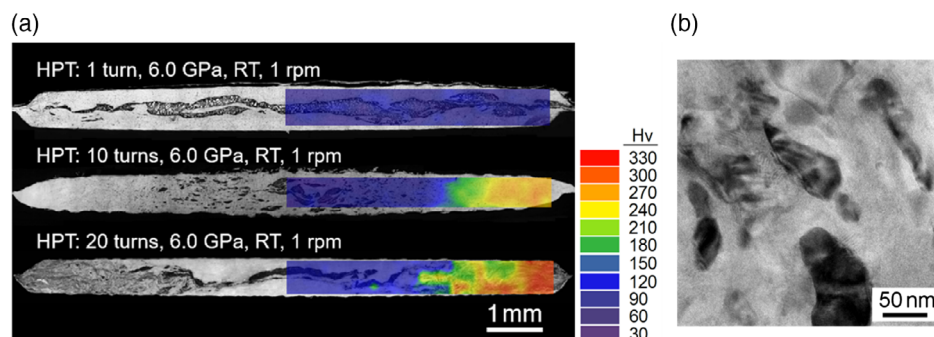


**Figure 2.** a) Overview of the cross sections and the corresponding hardness distributions for the Al–Mg disks having 10 mm diameter after HPT for, from the top, 1, 10, 20 turns at 6.0 GPa and b) a TEM micrographs taken at the disk edge after 20 HPT turns. Reproduced with permissions.<sup>[26]</sup> Copyright 2017, Wiley; Reproduced with permissions.<sup>[27]</sup> Copyright 2018, Wiley.

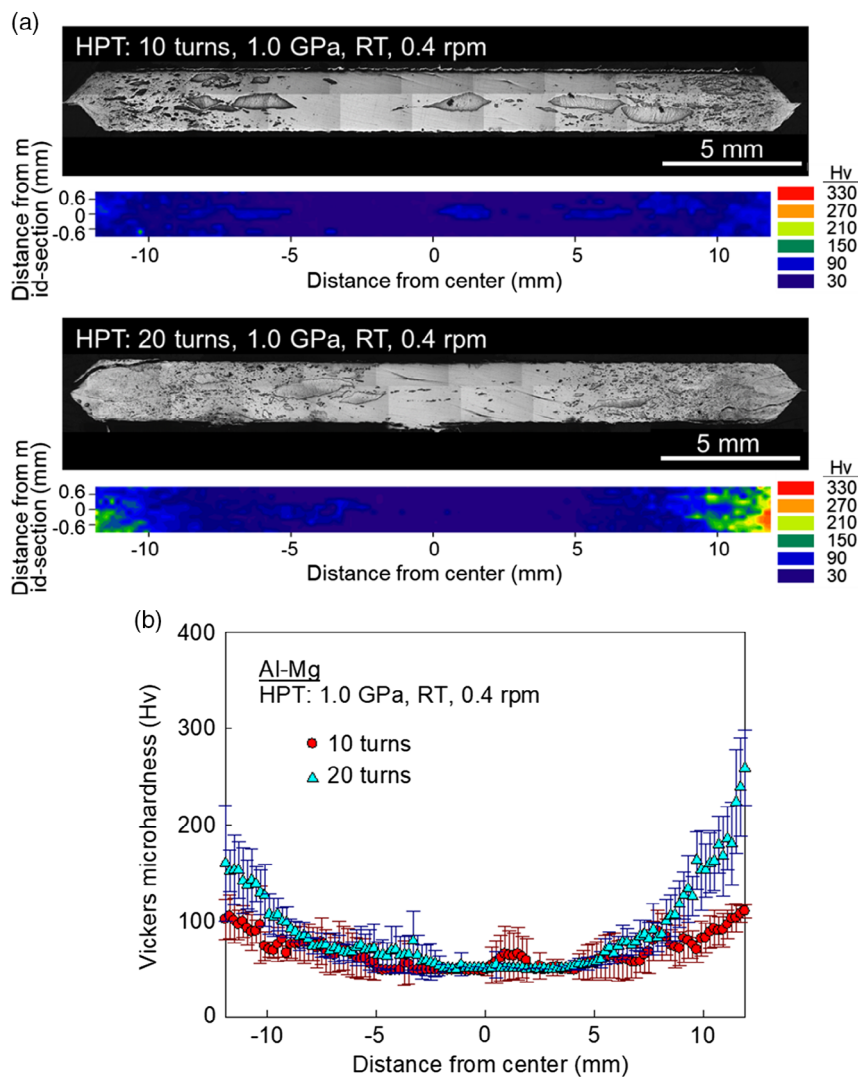


**Figure 3.** a) The cross-sectional micrographs and the corresponding hardness distributions as color-coded contour maps for the large Al–Mg disks with 25 mm diameter after processing by HPT for 10 turns (upper) and 20 turns (lower) under 1.0 GPa at 0.4 rpm and b) the hardness valuation with the standard error against the disk diameter for these two mechanically bonded Al–Mg disks.

diameter up to 20 HPT turns. This loss of Mg at the disk centers may be related to a significant change in the total disk thickness during the compression process and an early stage of concurrent torsion staining for the 25 mm diameter disks. It was observed in the present experiments that the mechanical bonding of the large disks having a total thickness of  $\approx 7.5$  mm demonstrates a large volume of metals flows out from the gap between the anvils so as to show the final thickness of  $\approx 2.4$  mm. It may cause a significant variation in the phase fractions of Al and Mg during the mechanical bonding of these phases, and further analysis is required in terms of the relationship between the sample dimension and the HPT parameters.

### 3.2. Microstructure and Phase Fraction

Microstructural analysis was conducted on the disk edge at  $r \approx 10$  mm after subjecting to the mechanical bonding by HPT

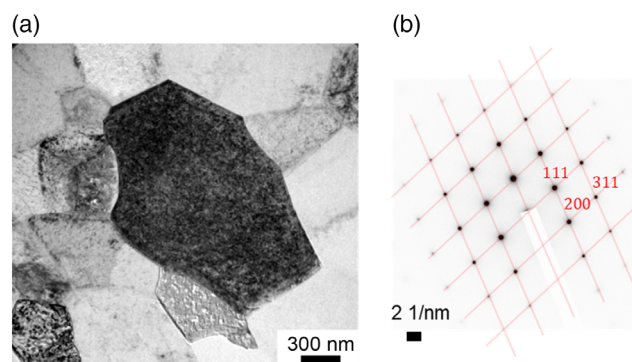


**Figure 4.** a) A representative TEM bright-field image and b) the SAED pattern taken at the disk edge at  $r \approx 10$  mm after subjecting to the mechanical bonding by HPT for 20 turns.



for 20 turns. **Figure 4a,b** shows a representative TEM bright-field image and the corresponding selected-area electron diffraction (SAED) pattern, respectively. The TEM micrograph shows the formation of equiaxed grains with clear grain boundaries. An average grain size of  $\approx 380$  nm was estimated, whereas several large grains with sizes over 500 nm existed as shown in **Figure 4a**. The SAED pattern in **Figure 4b** shows a typical spot distribution including 111, 200, and 311 indexes for an *f.c.c.* structure, thereby implying the presence of Al. There is no diffraction points indicating the *h.c.p.* Mg phase or any intermetallic phases within the measured area, whereas the examined region was too small to determine the actually existing phases at the edge region of the Al–Mg disk having 25 mm diameter after 20 HPT turns.

Accordingly, the phase fraction was examined by  $\mu$ XRD at three different regions of near-center, mid-radius, and edge of the Al–Mg disks with 25 mm diameter after HPT for 10 and 20 turns. The obtained XRD line profiles are shown in **Figure 5a,b** for the disks after 10 and 20 HPT turns, respectively, and the volume fractions of the phases computed by MAUD are shown in **Table 1** for the locations where more than one phase is detected by  $\mu$ XRD. The consistent strong peaks of an *f.c.c.* structure, such as 111, 200, 220, 311, and 222, are detected throughout the disk diameter of both disks after 10 and 20 turns. In addition, several Mg peaks were detected at the edge of the disk after 10 turns and at the mid-radius as well as the edge of the disk after 20 turns. In practice, as shown in **Table 1**, the disk after 10 turns includes Mg of  $\approx 1.5$  wt% at the disk edge and the Al–Mg disk after 20 turns holds the Mg phase of  $\approx 6.2$  and  $\approx 11.3$  wt% at the mid-radius and edge, respectively. It should be noted that the microstructural heterogeneity by torsion straining under the severe compressive pressure significantly affects the phase distributions of Al and Mg examined by  $\mu$ XRD at the different locations even at the equivalent distances from the disk centers. Nevertheless, the results provide a consistent trend of no Mg phase at near centers of the Al–Mg disks with 25 mm diameter after HPT for 10 and 20 turns.

### 3.3. Micromechanical Responses and Plasticity

Considering the microstructural evolution and increased hardness after the mechanical bonding of Al and Mg by HPT as

**Table 1.** The results on compositional analysis through MAUD based on the X-ray profile shown in **Figure 3**.

25 mm diameter disk	Location	Al [wt%]	Mg [wt%]
Al–Mg 10 turns	Edge	98.5 $\pm$ 0.1	1.5 $\pm$ 0.1
Al–Mg 20 turns	Edge	89.1 $\pm$ 0.1	11.3 $\pm$ 0.1
Al–Mg 20 turns	Mid-radius	93.8 $\pm$ 2.1	6.2 $\pm$ 2.1

shown in **Figure 3**, it is reasonable to evaluate the local mechanical properties at the disk edges of the Al–Mg system with 25 mm diameter. As suggested in an earlier report for measuring mechanical properties at a limited volume or local locations,<sup>[37]</sup> the present study uses nanoindentation for examining the micro-mechanical responses at the disk edges of the Al–Mg system after HPT. **Figure 6a** shows the representative load–displacement curves measured at four different strain rates for the edges at  $r = 10$  mm of the Al–Mg disks after HPT for 10 and 20 turns. Each curve represents an average mechanical response of at least 15 measurements at a strain rate. In fact, these 15 or more measurements involve an inevitable level of fluctuation at each nanoindentation strain rate due to the inhomogeneous distributions of phases and grain sizes in the Al–Mg system. It is apparent that the disk edge after HPT for 10 turns showed larger displacements than after 20 turns at all strain rates, thereby demonstrating improved hardness at the Al–Mg disk edges with an increasing number of HPT turns. Both Al–Mg disk edges exhibited clear dependence on the indentation strain rate.

Strain rate dependence of the micromechanical responses was evaluated and quantified by calculating the strain rate sensitivity,  $m$ , for the disk edges of the mechanically bonded Al–Mg system after HPT for 10 and 20 turns. In general, the value of  $m$  is determined by the following equation at a given strain,  $\epsilon$ , and absolute temperature,  $T$ , by considering Tabor's empirical prediction,<sup>[38]</sup> where the flow stress,  $\sigma_f$ , is equivalent to one-third of the indentation hardness,  $H$ , during fully plastic deformation at a constant strain rate,  $\dot{\epsilon}$ .

$$m = \left( \frac{\partial \ln \sigma_f}{\partial \ln \dot{\epsilon}} \right)_{\epsilon, T} = \left( \frac{\partial \ln (H/3)}{\partial \ln \dot{\epsilon}} \right)_{\epsilon, T} \quad (2)$$

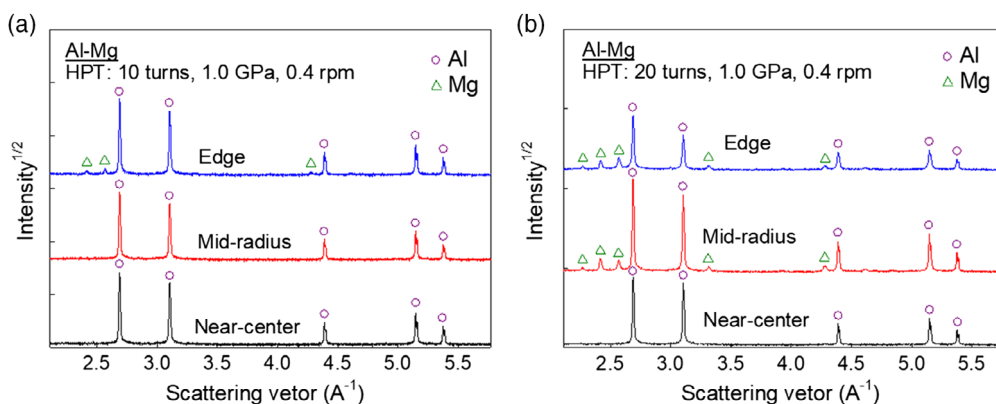


**Figure 5.** XRD line profiles examined by  $\mu$ XRD at three different regions of near-center, mid-radius, and edge of the Al–Mg disks with 25 mm diameter after HPT for a) 10 and b) 20 turns.

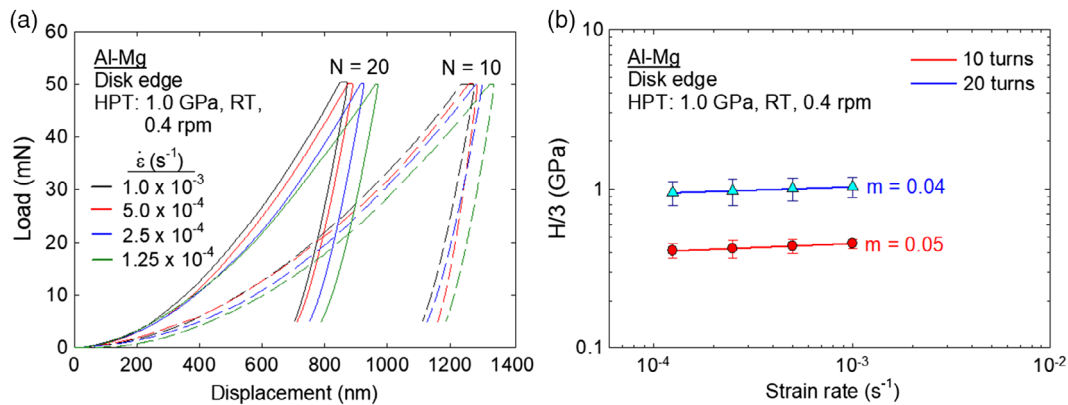


**Figure 6.** a) Representative load–displacement curves measured at four different strain rates and b) a logarithmic plot of  $H/3$  against  $\dot{\epsilon}$  for the for the disk edges at  $r = 10$  mm of the Al–Mg alloy after HPT for 10 and 20 turns.

Thus, the slope of the line in a logarithmic plot of  $H/3$  versus strain rate provides an estimated value of  $m$  for each sample, and the plot with the estimated  $m$  values is shown in Figure 6b for the edges of the Al–Mg disks with 25 mm diameter after 10 and 20 HPT turns. In this way, the strain rate sensitivity was calculated as  $m = 0.05$  after 10 turns and 0.04 after 20 turns under 1.0 GPa. Although there is no earlier data of the  $m$  value available for the HPT disk having 25 mm diameter, these estimated  $m$  values taken at  $r = 10$  mm for the Al–Mg disks are higher than 0.02 for the base material of the Al disk with 10 mm diameter when processed by HPT for 10 turns at 6.0 GPa<sup>[39]</sup> and are similar or slightly higher than 0.035–0.045 for the ZK60 disk with 10 mm diameter after 2 HPT turns measured by nanoindentation.<sup>[40]</sup> Thus, the mechanically bonded Al–Mg disks having 25 mm diameter show excellent plasticity with holding high hardness at the disk edges.

## 4. Discussion

### 4.1. Microstructural Differences with Increasing HPT Sample Size

Comparing the macroscale micrographs shown in Figure 2 for the 10 mm diameter disks and Figure 3 for the disks with 25 mm diameter, it is apparent that the achieved microstructures at the disk edges are different after equal numbers of HPT turns under consistent and torsional speed at the disk peripheries. The microstructural differences are further investigated using the line profiles measured by  $\mu$ XRD at near-center, mid-radius, and edges of the 25 mm diameter Al–Mg disks as shown in Figure 5. For comparison purposes, the earlier reported XRD line profiles are applied for the present analysis for the Al–Mg system with 10 mm diameter where XRD analysis was conducted at the overall disk edges after carefully removing the central regions after HPT for 10 turns<sup>[23]</sup> and 20 turns.<sup>[26]</sup>

The XRD data analysis estimates the lattice parameters of Al at the local regions. These estimated lattice parameters are used for computing the Mg solubility in the Al matrix at the measured local regions. In practice, the average Mg solubility,  $X_{\text{Mg}}$ , in at %, in the Al matrix can be estimated in the following form by

applying the lattice parameter of pure Al,  $a_0 = 4.049 \text{ \AA}$ , and the estimated lattice parameter,  $a$ .<sup>[41]</sup>

$$X_{\text{Mg}} = 9.045 \left( (a - a_0) / a_0 \right) \pm 0.003 \quad (3)$$

Moreover, the crystallite sizes and the microstrain were estimated by applying the Williamson–Hall method on the XRD profiles for the three different locations of near-center, mid-radius, and edge in the disks with 25 mm diameter and the edges of the disks with 10 mm diameter after HPT for 10 and 20 turns. Conventional Williamson–Hall plots are shown in Figure 7a,b for the 25 mm diameter Al–Mg system after HPT for 10 and 20 turns, respectively. The plots display full width at half maximum (FWHM),  $\Delta Q$ , of the XRD peak profiles against the scattering vector,  $Q$ , so that microstrain,  $\epsilon = \Delta Q / Q$ , and the crystallite size are given by the slope and an intercept at  $Q = 0$  of a fitted straight line, respectively, for each measurement location. A summary of the results is shown in Table 2.

Comparing the Al lattice parameters measured at three different locations within the disk having 25 mm diameter after HPT for 10 turns, a gradual expansion of lattices is observed from near-center to edge of the disk, thereby increasing lattice sizes with equivalent strain as calculated in Equation (1). This tendency is also demonstrated in the disk with 25 mm diameter after 20 HPT turns except all computed lattice parameters in the 20-turn disk are larger compared with those measured at the consistent locations in the 10-turn disk. This result is supported by the higher contents of Mg at the measured locations receiving higher equivalent strain, which is attributed to both increasing distances from the disk center and increasing numbers of HPT turns. On the contrary, the measured microstrain shows the highest at the mid-radius for both 10- and 20-turn disks with 25 mm diameter. This lowering of microstrain at the disk peripheries is caused by the significant free flow of the material volume during HPT processing due to the large sample dimension. Nevertheless, the smallest crystallite sizes of  $\approx 260$  nm and  $\approx 140$  nm are observed at the disk edges of the Al–Mg system with 25 mm diameter after HPT for 10 and 20 turns, respectively. Overall, these computed results show consistent changes in microstructure with increasing distances from disk centers as well as numbers of HPT turns and are in good agreement with

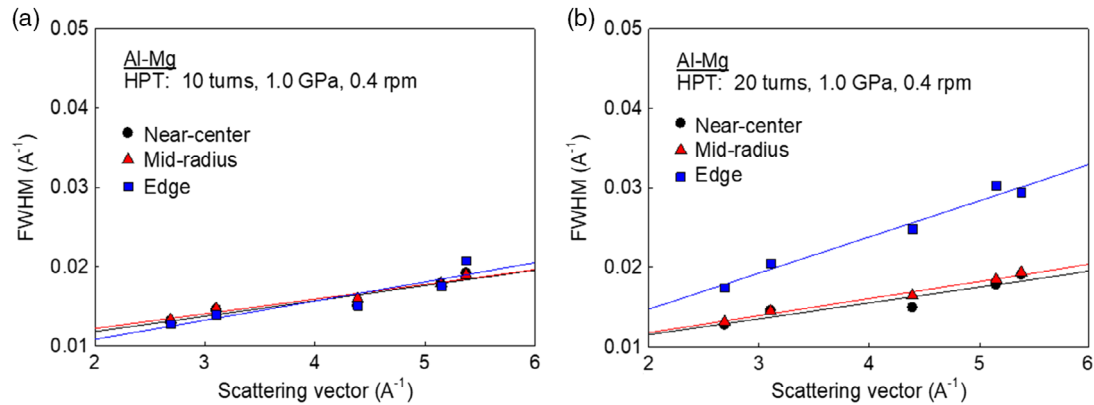


**Figure 7.** Williamson–Hall plots for the 25 mm diameter Al–Mg system after HPT for a) 10 and b) 20 turns under 1 GPa at 0.4 rpm.

**Table 2.** Summary of estimated lattice parameter of Al, concentration of Mg in the Al matrix, microstrain, and crystallite size for different measurement locations of center, mid-radius, and edge of the Al–Mg disks having 25 mm and 10 mm diameters processed by HPT for 10 and 20 turns. Earlier reported XRD data sets were used to estimate the parameters for the 10 mm diameter disks after HPT for 10<sup>[23]</sup> and 20 turns.<sup>[26]</sup>

	25 mm diameter disks						10 mm diameter disks [XRD data: 23,26]	
	10 turns			20 turns			10 turns	20 turns
	Near-center	Mid-radius	Edge	Near-center	Mid-radius	Edge	Edge	Edge
Lattice parameter (Å)	4.05066	4.05137	4.05200	4.05149	4.05204	4.05361	4.06296	4.06435
Mg contents (at%)	0.37	0.53	0.67	0.56	0.68	1.03	3.12	3.43
Microstrain	0.00795	0.00848	0.00600	0.00750	0.00565	0.00084	0.01500	0.00400
Crystallite size (nm)	325.1	339.2	260.2	315.0	292.3	138.1	78.9	47.3

the enhanced hardness at the Al–Mg disk peripheries as shown in Figure 3. It is important to note that the measured Mg contents in the Al–Mg system having 25 mm diameter are below the maximum Mg solubility of  $\approx 1.6$  at% (equivalent to  $\approx 1.4$  wt%) in Al at room temperature, and thus there is no evidence for the formation of supersaturated solid solutions in the mechanically bonded Al–Mg disks having 25 mm diameter.

A reasonable result was obtained for the disk edges of the Al–Mg system with 10 mm diameter where lattice parameter of Al, the Mg contents, and microstrain increase and crystallite size decreases with increasing numbers of HPT turns from 10 to 20. The estimated crystallite sizes for the disks having 10 mm diameter are reasonably consistent with the reported grain sizes of 90<sup>[23]</sup> and 60 nm<sup>[26]</sup> after 10 and 20 HPT turns, respectively, which are directly measured from the TEM micrographs. Comparing the results between the two different HPT sample sizes, it is apparent that the edges of the disks with 10 mm diameter demonstrate dramatic changes in microstructure, whereas torsional speed at the disk edges is equivalent for all disks having different sample sizes. This finding is in good agreement with a recent report demonstrating a comparison of the hardness variation along the normalized disk radius between three different disk diameters of 8, 30, and 60 mm of Cu after HPT for 5–10 turns.<sup>[32]</sup> A small Cu disk with 8 mm diameter showed high hardness throughout the normalized radius, while lowering hardness was recorded throughout the normalized radius with increasing sample sizes. The report interpreted the result by considering an increased deformation temperature

during HPT processing for the large HPT samples, although the deformation speed was significantly reduced for processing the large samples to avoid the heat generation for the large-sized specimens. Moreover, it should be noted that the difference in compressive pressure must be another critical factor for demonstrating such difference in the microstructural evolution for the Al–Mg alloy system. This is well confirmed in an earlier report with estimating a modified diffusion coefficient of Mg into Al where high imposed hydraulic pressure of HPT leads to an acceleration of Mg diffusion into Al at room temperature.<sup>[23]</sup>

#### 4.2. Interpretation of Hardness Evolution in the Al–Mg System

One of earlier studies evaluating the hardness evolution of ultrafine-grained materials during HPT demonstrated that the measured microhardness values of an austenitic steel show a close correlation with the accumulated equivalent strain as calculated in Equation (1).<sup>[42]</sup> Thereafter, numerous studies followed the approach of evaluating the hardness evolution with increasing equivalent strain for a variety of materials, and a summary of the hardness behavior for the HPT-processed metals and alloys was reported with a special emphasis on three separate models of hardness evolution, which are dependent upon the nature of microstructural recovery in the materials.<sup>[43]</sup> Within the constructed models, most of commercial purity metals and simple alloys show the standard model of hardness development with

increasing equivalent strain where the hardness increases quickly in an early stage of deformation and ultimately saturates at a reasonably high equivalent strain of 20–50. This type of hardness behavior denotes materials in the absence of any microstructural recovery,<sup>[44]</sup> and earlier examination showed that the base materials of both the commercial purity Al<sup>[45]</sup> and the ZK60 magnesium alloy<sup>[34]</sup> used in the present study for the mechanical bonding exhibited the consistent hardness behavior.

Accordingly, the mechanically bonded Al–Mg system having 10 and 25 mm diameters is evaluated with the same approach where the measured Vickers microhardness values are plotted against equivalent strain. Applying the fact that the large volume of materials flows out during the compression stage, the present calculations used the disk thicknesses of  $h = 2.4$  mm for the large Al–Mg system having 25 mm diameter and  $h = 0.7$  mm for the system with 10 mm diameter after HPT for 10 and 20 turns. The results of the hardness value versus equivalent strain are displayed in **Figure 8** for the Al–Mg system disks having 10 and 25 mm diameters. It should be noted that equivalent strain is shown in logarithmic scale to cover a wide range of the value.

There are three unique features shown in **Figure 8**. First, all disks show a consistent trend of hardness behavior outlining an exponential increase of hardness with increasing equivalent strain. Specifically, low hardness was recorded at low values of equivalent strain, and it is followed by an exponential growth of hardness with increasing equivalent strain. Moreover, the increased hardness demonstrates no saturation in the present measurements for both 10 and 25 mm diameter disks through HPT for 20 turns. This significant increase in hardness is attributed to a severe phase mixture of the dissimilar metals during the grain refinement process.<sup>[23]</sup> In practice, for the disks with 10 mm diameter, the recorded high hardness involves the formation of intermetallic phases at the disk edges in the Al–Mg system after HPT for 10–20 turns.<sup>[23,26]</sup> Second, the disks having 25 mm diameter show lower hardness than the disks having 10 mm diameter at any equivalent strain. This result may be affected by two different points: different HPT processing pressure leading to a different level of severe plastic deformation<sup>[46]</sup> and an axial heterogeneity of hardness which often significant in large height samples.<sup>[30–32]</sup> Third, a dramatic increase of

hardness starts at different levels of equivalent strain for the Al–Mg system, and it depends not only on the disk diameter but also on the total number of HPT turns. In practice, the disks having different diameters of 10 mm and 25 mm after 10 HPT turns showed an apparent hardness increase at an equivalent strain of  $\approx 100$ , whereas such hardness increase was observed at an equivalent strain of  $>200$  for the disks with 10 and 20 mm diameters after 20 HPT turns. This difference may be related to the inevitable heat generation that will occur highly with increasing numbers of HPT turns. The accumulated heat energy promotes microstructural recovery leading to the hardness suppression in the Al–Mg disks.

It should be noted that the deformation mechanisms for the mechanically bonded Al–Mg disks after HPT for 5 and 10 turns were well estimated mainly by applying the Hall–Petch strengthening with partial but critical contributions of solution strengthening due to the solutionization of Mg atoms into the Al phase and precipitation hardening by considering the presence of intermetallic phases as precipitates.<sup>[23]</sup> Applying the described mechanisms, it is reasonable to conclude that the Al–Mg system with 25 mm diameter shows such lower hardness after 10 and 20 turns in comparison with the 10 mm diameter disks because of larger grain sizes and less content of Mg into Al as shown in **Table 2** and no formation of intermetallic compound as shown in **Figure 5**.

The present hardness evaluation shows for the first time a hardness model for an Al–Mg alloy system when synthesized by the mechanical bonding through HPT. Processing by HPT has been utilized for the mechanical bonding of several different combinations of dissimilar bulk metals with significant grain refinement. These reported metal combinations include Al–Cu,<sup>[19–22]</sup> Al–Mg,<sup>[23–27]</sup> Al–Fe,<sup>[27]</sup> Al–Ti,<sup>[27]</sup> Cu–Ta,<sup>[47]</sup> Cu–ZnO,<sup>[48]</sup> Mg–Zn,<sup>[49]</sup> Fe–V,<sup>[50,51]</sup> V–10Ti–5Cr/Zr–2.5Nb<sup>[52]</sup> systems. Considering the present results showing the improvement in both hardness and plasticity in the HPT-induced mechanically bonded Al–Mg system in comparison with the base metals, this processing approach demonstrates a significant contribution to developments in the synthesis of advanced materials and in current diffusion bonding, welding, and mechanical joining technologies.

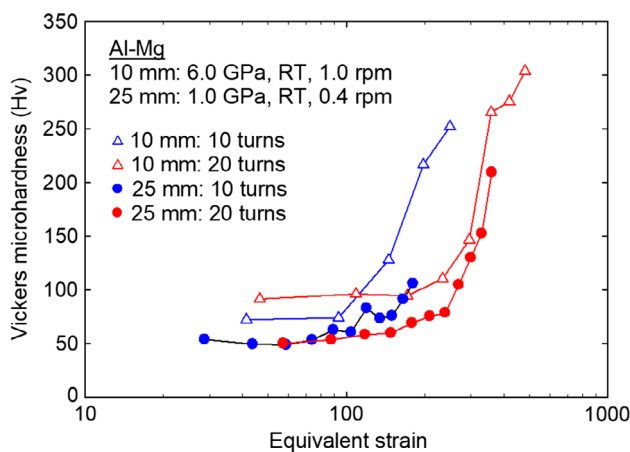


**Figure 8.** Variation of microhardness with equivalent strain for the Al–Mg system disks having 10 and 25 mm diameter.

## 5. Conclusions

- 1) The mechanical bonding of separate Al and Mg disks having 25 mm diameter was demonstrated through HPT under 1.0 GPa at room temperature for 10 and 20 turns at 0.4 rpm. The influence of scaling up of the sample dimension was evaluated by comparison with the mechanically bonded Al–Mg disks with 10 mm diameter after HPT for 10 and 20 turns at 6.0 GPa and 1 rpm.
- 2) The processed Al–Mg disks having 25 mm diameter show a general hardness distribution where low hardness appears around the disk centers, but it increases at the disk peripheries. The highest recorded Vickers microhardness of  $\approx 250$  was observed at the disk edge after 20 HPT turns where an average grain size of 380 nm was observed by TEM. The  $\mu$ XRD and analysis MAUD revealed the microstructural heterogeneity by torsion straining under the severe compressive pressure.
- 3) The Al–Mg system after the mechanical bonding



through HPT demonstrated reasonable plastic stability at the disk edges with the strain rate sensitivity of  $m = 0.05$  after 10 turns and 0.04 after 20 turns under 1.0 GPa. In addition to the improved hardness, there is excellent plasticity at the edges of the mechanically bonded Al–Mg system. 4) Microstructural heterogeneity in the mechanically bonded Al–Mg disks with 25 mm diameter was confirmed through MAUD analysis by computing an increase in lattice parameter of Al due to high contents of Mg in the Al phase and a decrease in crystallite sizes at the locations receiving higher equivalent strain, which is attributed to both increasing distance from the disk center and increasing numbers of HPT turns. 5) The Al–Mg system with 10 and 25 mm diameters shows a consistent trend of hardness evolution outlining an exponential increase of hardness with increasing equivalent strain. A dramatic increase of hardness depends not only on the disk diameter but also on the total number of HPT turns. However, severe microstructural mixture can be observed in the small disk since the large disk may generate an inevitable temperature rise promoting the microstructural recovery within the sample having large diameter during HPT under a consistent rotational speed at the disk peripheries.

## Acknowledgements

This study was supported by the National Science Foundation of the United States under grant no. DMR-1810343 (M.K. & J.K.H.). The work at Hanyang University was supported by the National Research Foundation of Korea (NRF) grants funded by the Ministry of Science and ICT, grant nos. 2015R1A5A1037627 and 2017R1A2B4012255 (J.M.P. & J.i.).

## Conflict of Interest

The authors declare no conflict of interest.

## Keywords

grain refinement, heterostructures, high-pressure torsion, mechanical bonding, nanoindentations

Received: August 10, 2019

Revised: October 8, 2019

Published online: November 8, 2019

- [1] R. Z. Valiev, Y. Estrin, Z. Horita, T. G. Langdon, M. J. Zehetbauer, Y. T. Zhu, *JOM* **2006**, 58, 33.
- [2] R. Z. Valiev, Y. Estrin, Z. Horita, T. G. Langdon, M. J. Zehetbauer, Y. T. Zhu, *JOM* **2016**, 68, 1216.
- [3] A. P. Zhilyaev, T. G. Langdon, *Prog. Mater. Sci.* **2008**, 53, 893.
- [4] A. P. Zhilyaev, A. A. Gimazov, G. I. Raab, T. G. Langdon, *Mater. Sci. Eng., A* **2008**, 486, 123.
- [5] K. Edalati, Y. Yokoyama, Z. Horita, *Mater. Trans.* **2010**, 51, 23.
- [6] M. I. Abd El Aal, E. Y. Yoon, H. S. Kim, *Mater. Sci. Eng., A* **2013**, 560, 121.
- [7] M. M. Castro, P. H. R. Pereira, A. Isaac, R. B. Figueiredo, T. G. Langdon, *J. Alloys Compd.* **2019**, 780, 422.
- [8] A. V. Korznikov, I. M. Safarov, D. V. Laptionok, R. Z. Valiev, *Acta Metall. Mater.* **1991**, 39, 3193.
- [9] V. V. Stolyarov, Y. T. Zhu, T. C. Lowe, R. K. Islamgaliev, R. Z. Valiev, *Mater. Sci. Eng., A* **2000**, 282, 78.
- [10] X. Sauvage, P. Jessner, F. Vurpillot, R. Pippan, *Scr. Mater.* **2008**, 58, 1125.
- [11] K. Kaneko, T. Hata, T. Tokunaga, Z. Horita, *Mater. Trans.* **2009**, 50, 76.
- [12] K. Edalati, Z. Horita, H. Fujiwara, K. Ameyama, *Metall. Mater. Trans. A* **2010**, 41, 3308.
- [13] A. Bachmaier, M. Kerber, D. Setman, R. Pippan, *Acta Mater.* **2012**, 60, 860.
- [14] J. M. Cubero-Sesin, Z. Horita, *Mater. Sci. Eng., A* **2012**, 558, 462.
- [15] Y. Zhang, S. Sabbaghianrad, H. Yang, T. D. Topping, T. G. Langdon, E. J. Lavernia, J. M. Schoenung, S. R. Nutt, *Metall. Mater. Trans. A* **2015**, 46, 5877.
- [16] A. P. Zhilyaev, G. Ringot, Y. Huang, J. M. Cabrera, T. G. Langdon, *Mater. Sci. Eng., A* **2017**, 688, 498.
- [17] Y. Huang, P. Bazarnik, D. Wan, D. Luo, P. H. R. Pereira, M. Lewandowska, J. Yao, B. E. Hayden, T. G. Langdon, *Acta Mater.* **2019**, 164, 499.
- [18] B. Wan, W. Chen, T. Lu, F. Liu, Z. Jiang, M. Mao, *Resour., Conserv. Recycl.* **2017**, 125, 37.
- [19] K. Oh-ishi, K. Edalati, H. S. Kim, K. Hono, Z. Horita, *Acta Mater.* **2013**, 61, 3482.
- [20] O. Bouaziz, H. S. Kim, Y. Estrin, *Adv. Eng. Mater.* **2013**, 15, 336.
- [21] J.-K. Han, D. K. Han, G. Y. Liang, J.-I. Jang, T. G. Langdon, M. Kawasaki, *Adv. Eng. Mater.* **2018**, 20, 1800642.
- [22] V. N. Danilenko, S. N. Sergeev, J. A. Baimova, G. F. Korznikova, K. S. Nazarov, R. K. Khisamov, A. M. Glezer, R. R. Mulyukov, *Mater. Lett.* **2019**, 236, 51.
- [23] B. Ahn, A. P. Zhilyaev, H.-J. Lee, M. Kawasaki, T. G. Langdon, *Mater. Sci. Eng., A* **2015**, 635, 109.
- [24] M. Kawasaki, B. Ahn, H.-J. Lee, A. P. Zhilyaev, T. G. Langdon, *J. Mater. Res.* **2016**, 31, 88.
- [25] B. Ahn, H.-J. Lee, I.-C. Choi, M. Kawasaki, J.-I. Jang, T. G. Langdon, *Adv. Eng. Mater.* **2016**, 18, 1001.
- [26] J.-K. Han, H.-J. Lee, J.-I. Jang, M. Kawasaki, T. G. Langdon, *Mater. Sci. Eng., A* **2017**, 684, 318.
- [27] M. Kawasaki, J.-K. Han, D.-H. Lee, J.-I. Jang, T. G. Langdon, *J. Mater. Res.* **2018**, 33, 2700.
- [28] R. Z. Valiev, Y. V. Ivanisenko, E. F. Rauch, B. Baudalet, *Acta Mater.* **1996**, 44, 4705.
- [29] F. Wetscher, A. Vorhauer, R. Stock, R. Pippan, *Mater. Sci. Eng., A* **2004**, 809, 387.
- [30] Z. Horita, T. G. Langdon, *Scr. Mater.* **2008**, 58, 1029.
- [31] A. Hohenwarter, A. Bachmaier, B. Gludovatz, S. Scherlauer, R. Pippan, *Int. J. Mater. Res.* **2009**, 100, 1653.
- [32] A. Hohenwarter, R. Pippan, *Metall. Mater. Trans. A* **2019**, 50, 601.
- [33] L. Lutterotti, *Nucl. Instrum. Methods Phys. Res., Sect. B* **2010**, 268, 334.
- [34] H.-J. Lee, S. K. Lee, K. H. Jung, G. A. Lee, B. Ahn, M. Kawasaki, T. G. Langdon, *Mater. Sci. Eng., A* **2015**, 630, 90.
- [35] Y. Huang, M. Kawasaki, T. G. Langdon, *J. Mater. Sci.* **2013**, 48, 4533.
- [36] Y. Huang, M. Kawasaki, T. G. Langdon, *J. Mater. Sci.* **2014**, 49, 3146.
- [37] M. Kawasaki, B. Ahn, P. Kumar, J.-I. Jang, T. G. Langdon, *Adv. Eng. Mater.* **2017**, 19, 1600578.
- [38] S. Shim, J.-I. Jang, G. M. Pharr, *Acta Mater.* **2008**, 56, 3824.
- [39] M. Kawasaki, S. H. Jung, J.-M. Park, J. Lee, J.-I. Jang, J.-K. Han, *Adv. Eng. Mater.*, <https://doi.org/10.1002/adem.201900483>, unpublished.
- [40] I.-C. Choi, D.-H. Lee, B. Ahn, K. Durst, M. Kawasaki, T. G. Langdon, J.-I. Jang, *Scr. Mater.* **2015**, 94, 44.
- [41] M. Schoenitz, E. L. Dreizin, *J. Mater. Res.* **2003**, 18, 1827.
- [42] A. Vorhauer, R. Pippan, *Scr. Mater.* **2004**, 51, 921.
- [43] M. Kawasaki, *J. Mater. Sci.* **2014**, 49, 18.

- [44] K. Edalati, T. Fujioka, Z. Horita, *Mater. Trans.* **2009**, *50*, 44.
- [45] M. Kawasaki, S. N. Alhajeri, C. Xu, T. G. Langdon, *Mater. Sci. Eng., A* **2011**, *529*, 345.
- [46] A. P. Zhilyaev, S. Lee, G. V. Nurislamova, R. Z. Valiev, T. G. Langdon, *Scr. Mater.* **2001**, *44*, 2753.
- [47] N. Ibrahim, M. Peterlechner, F. Emeis, M. Wegner, S. V. Divinski, G. Wilde, *Mater. Sci. Eng., A* **2017**, *685*, 19.
- [48] Y. Qi, A. Kosinova, A. R. Kilmametov, B. B. Straumal, E. Rabkin, *Mater. Charact.* **2018**, *145*, 389.
- [49] D. Hernández-Escobar, Z. U. Raman, H. Yilmazer, M. Kawasaki, C. J. Boehlert, *Phil. Mag.* **2019**, *99*, 557.
- [50] S. O. Rogachev, R. V. Sundeev, V. M. Khatkevich, *Mater. Lett.* **2016**, *173*, 123.
- [51] S. O. Rogachev, S. A. Nikulin, A. B. Rozhnov, V. M. Khatkevich, T. A. Nechaykina, M. V. Gorshenkov, R. V. Sundeev, *Metall. Mater. Trans. A* **2017**, *48*, 6091.
- [52] S. O. Rogachev, R. V. Sundeev, N. Y. Tabachkova, *Mater. Lett.* **2019**, *234*, 220.